Received: 12 March 2024 | Revised: 26 April 2024 | Accepted: 18 May 2024

DOI: 10.1002/amp2.10179

RESEARCH ARTICLE

JOURNAL OF ADVANCED MANUFACTURING AND PROCESSING WILEY

Enhancing decanter centrifuge process design with data-driven material parameters in multi-compartment modeling

Ouwen Zhai | **Niklas Ehret** | **Frank Rhein** | **Marco Gleiss**

Institute of Mechanical Process Engineering and Mechanics, Karlsruhe Institute of Technology, Karlsruhe, Germany

Correspondence
Ouwen Zhai, Institute of Mechanical Process Engineering and Mechanics, Karlsruhe Institute of Technology, Karlsruhe 76131, Germany.
Email: ouwen.zhai@kit.edu

Funding information
German Federation of Industrial Research Associations (AiF), Grant/Award Number: 21638N; Federal Ministry for Economic Affairs and Climate Action

Abstract

Predicting the separation performance of decanter centrifuges is challenging due to dynamic events within the apparatus. Current methods for designing decanter centrifuges rely on simplified models, often leading to inaccuracies. Consequently, manufacturers must perform time-intensive pilot scale experiments to derive their own correction factors. Growing computing power sparks interest in alternative modeling strategies. Grey box models (GBM) combine mechanistic white box models (WBM) and data-driven black box models (BBM), with the optimal structure (parallel or serial) varying by application. For modeling decanter centrifuges, we propose a serial GBM that comprises an artificial neural network that outputs unknown material parameters into a first-principle multi-compartment model. Comparing this approach to alternative data-driven modeling strategies (pure BBM, parallel GBM), we conclude that the serial GBM excels in terms of extrapolation, prediction ability, and transparency while also enabling a better comprehension of the separation process.

KEYWORDS

artificial neural network, decanter centrifuge, grey box modeling, machine learning, solid–liquid separation

1 | INTRODUCTION

Continuous solid bowl centrifuges, such as decanter centrifuges, are widely used in food, chemical and mineral processing industries and play a crucial role in processes such as clarification, dewatering, and solid–liquid separation. For instance, decanter centrifuges play a pivotal role in reducing waste and environmental impact by separating harmful pollutants from water during wastewater treatment. The separation efficiency of solid bowl centrifuges is heavily dependent on their design and the selection of process parameters. Achieving the desired separation efficiency and dryness of the sediment is of significant importance for the product quality and the energy consumption of subsequent process steps, such as thermal drying. Inadequate dimensioning and process conditions can lead to poor separation performance and increased energy consumption. A cost-effective operation is typically achieved based on expert knowledge and process understanding gained over time. However,

predicting the effect of individual process parameters on the separation result can be difficult due to the complex interplay of the process parameters and centrifuge geometry. This makes the dimensioning, scale-up, and efficient operation of solid bowl centrifuges challenging.

As the technological landscape evolves, there is a growing interest in the use of predictive models to address challenges related to dimensioning, optimizing operational efficiency, and reducing energy consumption. There are numerous modeling approaches to predict the separation outcome in decanter centrifuges. Basic steady-state models, including the sigma theory by Ambler,[1] are still commonly used. However, these models neglect dynamic events within the apparatus, such as the hindered settling, the build-up and consolidation of the sediment. Consequently, manufacturers must conduct time-consuming pilot scale experiments and derive their own empirical factors to account for model inaccuracies. Therefore, it is of great significance to develop models which are more reliable and accurate.

On one hand, the use of numerical models has become more prevalent due to the ever-increasing computing power. On the other hand, the increasing use of sensors in machines allows for the collection of large amounts of process data, such as volumetric flow rate, solids content, and particle size distribution. This has led to an increased interest in data-driven models.

Generally, the models can be categorized into three types: White box models (WBMs), black box models (BBMs), and grey box models (GBMs). WBMs are mechanistic first-principle models that typically use prior knowledge of the process in form of mass, energy, or momentum balances. Calculations done by WBMs are completely transparent. The complexity of WBMs range from simple equations to nonlinear partial differential equations. While computational fluid dynamics (CFD) methods allow for fully resolved flow simulations of decanter centrifuges,[2] the computation time is significant, which makes them unsuitable for real-time applications, such as model-predictive control. On the other hand, so-called real-time models simplify complex systems through assumptions, reducing the computational effort significantly. Gleiß et al.[3] present a real-time first-principle model for counter-current decanter centrifuges by discretizing the unrolled helical path of the conveyor into a defined number of compartments. The approach can describe the settling behavior of the particles and the sediment build-up in the cylindrical part of a decanter centrifuge by coupling the residence time behavior of the decanter centrifuge with empirical material functions. Menesklou et al.[4] extended the model by including the conical part of the decanter centrifuge, which plays a crucial role in the dewatering and transport behavior of the sediment. Furthermore, Menesklou et al.[5] conducted experiments using various calcium carbonate water suspensions and a decanter centrifuge of laboratory and industrial scale to validate the real-time model. Although the predictions are reliable overall, certain phenomena, such as local flow effects at deeper pool depth, are not considered in the model, leading to inaccuracies for specific process conditions. Bai et al.[6,7] present a similar model to predict the separation and classification outcome of decanter centrifuges. The study analyzes different flow patterns, including plug flow, parabolic flow, and a flow pattern that considers backflow near the bowl wall and sediment surface. The authors conclude that the most accurate flow pattern is the one that considers the backflow. However, the consolidation behavior of compressible material is not considered in their model.

BBMs, such as artificial neural networks (ANNs), can be used without prior knowledge of the process. They require a sufficient amount of process data for the training procedure. As data-driven models, the prediction quality depends mainly on the quantity and quality of the available input data. Generally, sparse or noisy data results in unreliable predictions. BBMs also tend to perform poorly in extrapolation. Jiménez et al.[8,9] use an ANN to optimize the olive oil elaboration process in a decanter centrifuge. In their studies, the input parameters of their ANN comprised of process parameters such as flow rate, temperature, and dilution ratio of the feed. Meanwhile, the output parameters are the fat content and the moisture in the olive pomace. While the authors demonstrate that the ANN makes reasonable predictions for this particular application, the influence of other important process parameters of a decanter centrifuge, such as the rotational speed of the bowl and the differential speed of the conveyor, are not considered.

Another modeling approach involves combining a WBM and a BBM to create a hybrid model, also known as grey box model (GBM). In general, the WBM and the BBM can be connected in a serial or in a parallel way. In a parallel arrangement, the BBM learns the mismatch between the WBM and experimental data to consider unmodeled effects, non-linearity or dynamic behavior.[10–15] Various approaches exist to fuse the outputs of the BBM and WBM, including the most commonly used approach of simple superposition. Menesklou et al.[12] demonstrate an example of a parallel GBM for modeling decanter centrifuges by combining the previously mentioned real-time model[3,4] with an ANN in their study. The ANN functions as an estimator of the deviation between the WBM and the experimental data. Results show that the predictions of the parallel GBM are considerably more accurate compared to that of the pure WBM. In a serial arrangement, the BBM

estimates non-measurable intermediate parameters of the WBM that cannot be directly measured.[13,16–24] Psichogias et al.[25] use a GBM with a serial arrangement for modeling and model-based control of a fed-batch bioreactor. In their approach, an ANN estimates an unknown kinetic parameter, which is subsequently fed into the component mass balances of the first-principle model. According to the authors, this approach leads to less model complexity required and an improved performance in comparison to a pure ANN. Choosing the optimal structure for a hybrid model is a challenging task as it is highly dependent on the specific application. Complicating matters further, the choice of the BBM can also have a large impact on model performance. Rhein et al.[26] and Chen et al.[27] propose hybrid modeling frameworks, and evaluate the performance of various model structures, including a parallel GBM, a serial GBM and a pure BBM using different Machine Learning algorithms for their application. Rhein et al.[26] conclude that the serial approach outperforms the other model structures in terms of prediction performance, interpolation ability, and model transparency, proving that it is the optimal choice for their case study of modeling a hetero-agglomeration process. Chen et al.[27] propose a framework for identifying plant-model mismatch and applying hybrid modeling using a first-order reactor model. They demonstrate, with two pharmaceutical unit operation case studies, that hybrid modeling increases the accuracy of the reactor model, while the optimal model structure varies depending on the case. Bradley et al.[28] review recent contributions in three areas of dynamic process modeling: Hybrid modeling, Physics-Informed Machine Learning, and Model Calibration. They discuss the pros and cons of each area and conclude that, in general, hybrid models outperform purely data-driven models. For optimization applications, they suggest using hybrid modeling based on mechanism estimation. This approach demonstrates better extrapolation ability and generalizability, although the authors emphasize the importance of avoiding excessive influence of the data-driven component on the model output and preserving the interpretability of the model.

In this study, we introduce a GBM with a serial arrangement to predict the separation process in a counter-current decanter centrifuge, incorporating a posteriori knowledge into the real-time model developed by Gleiß et al.[3] and Menesklou et al.[4] The GBM considers the fundamental physical principles of the separation process while incorporating empirical data to address uncertainties associated with the material functions within the WBM. Additionally, we compare the performance of the serial GBM with that of the pure WBM, a pure BBM, and a parallel GBM for predicting the separation outcome of a laboratory scale decanter centrifuge under various operating conditions. This is the first time that a comprehensive analysis of different model structures for decanter centrifuges and their ability to extrapolate is carried out.

2 | MODELING APPROACHES

2.1 | Black box model: Artificial neural network

There are numerous Machine Learning methods available, each with its own advantages and disadvantages. One widely used method is the artificial neural network (ANN), which is inspired by the architecture of the brain and acts as a data-based universal function approximator.[29] ANNs consist of an input layer, at least one hidden layer, and an output layer, connected by weighted connections. During training, the weights are adjusted to minimize loss. The parameters that regulate the structure of the ANN, such as the learning rate, the number of neurons, and the number of layers, are referred to as hyperparameters (HP) and have to be tuned to the available data. A loss function, such as the root mean squared error (RMSE), is used to evaluate the model performance:

$$\mathrm{RMSE} = \sqrt{\mathrm{MSE}} = \sqrt{\frac{1}{N}\sum_{i}^{N}\left(Y_i - \widehat{Y}_i\right)^2} \tag{1}$$

with the prediction $\widehat{Y}$, the true value Y, and the total number of samples N. In order to prevent poor generalization, regularization techniques are important to avoid overfitting resulting from high model complexity and variance. Ridge regression[30] is a method to prevent individual weights from becoming overly dominant relative to other weights by adding a penalty term to the loss function. Using the ridge regression in combination with the mean squared error (MSE), the following modified loss function is obtained:

$$\underbrace{\frac{1}{N}\sum_{i}^{N}\left(Y_i - \widehat{Y}_i\right)^2}_{\text{loss function}} + \underbrace{\lambda\sum_{m}^{M}\sum_{l}^{L} w_{m,l}^2}_{\text{penalty term}} \quad \lambda \in [0,\infty) \tag{2}$$

where $w_{m,l}$ is the weight of layer L and connection M and λ controls the strength of the penalty on large weights. Aggarwal[31] gives a more in depth overview of the theoretical concepts and practical applications of ANNs.

2.2 | White box model: Multi-compartment model of decanter centrifuges

A schematic depiction of a counter-current decanter centrifuge is shown in Figure 1. The feed, with a specified solids concentration, particle size distribution and volumetric flow rate, enters the decanter centrifuge through an inlet pipe. Due to the rotation of the bowl, centrifugal forces are generated, causing the denser phase to settle towards the inner wall of the bowl. When higher density particles are dispersed in a lower density liquid phase, the settled particles accumulate and form a sediment. To transport the sediment, a screw conveyor rotates at a different speed relative to the rotational speed of the bowl. This introduces shear forces into the sediment, causing the sediment to move along the conical part of the bowl until it is discharged. In a counter-current decanter centrifuge, the clarified suspension, known as centrate, flows in the opposite direction over a weir. Stahl[33] describes the basic operation of decanter centrifuges and how various process parameters affect the separation result in detail.

For this work, a real-time first-principle process model presented in the work of Gleiß et al.[3,32] and Menesklou et al.[4] is used as the WBM. The geometry of the decanter centrifuge, the process parameters, and the material parameters are necessary inputs for the model. Its output includes the filling capacity of the centrifuge, the solids content and the particle size distribution of the centrate and sediment. This study focuses on the solids content since it is the most easily validated. In the WBM, the helical conveyor channel is first unrolled and then discretized into a predefined number of compartments, which are linked by mass balances and represent the residence time behavior of the decanter centrifuge. The discretization is illustrated in Figure 1. Due to the vastly different material behavior of the suspension and the sediment, each compartment is further divided into a suspension zone and a sediment zone. A material-specific solids fraction volume fraction, also known as the gel point $\phi_{v,\mathrm{gel}}$, characterizes the abrupt transition from suspension to sediment and describes the solids concentration at which first particle-particle contacts occur. The gel point is determined empirically according to Stickland[34] and Spelter.[35] Empirical material functions are utilized for describing the settling behavior in the settling zone. To accurately describe the settling dynamics in the apparatus, the hindered settling has to be considered. In the case of highly concentrated liquid suspensions, the momentum exchange between the particles and the fluid leads to a reduced settling velocity compared to the Stokes' settling velocity[36] u_{Stokes}. In order to account for this reduced settling velocity, a modified hindered settling function $H(\phi_v)$ according to Micheals et al.[37] is used:

$$H(\phi_v) = \frac{u}{u_{\mathrm{Stokes}}} = r_1\left(1 - \frac{\phi_v}{r_2}\right)^{r_3} \tag{3}$$

Here, the hindered settling velocity u depends on the solids volume fraction ϕ_v and the empirical material-specific parameters r_1, r_2, r_3, which are experimentally determined for each material by an analytical centrifuge LUMiSizer (LUM GmbH). A detailed description of the measurement principle and the methodology is given by

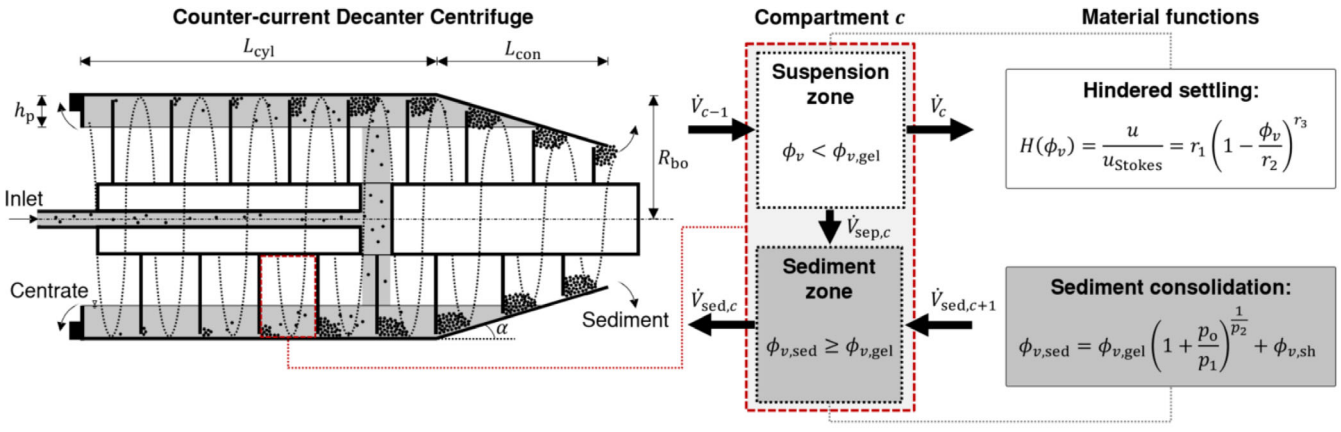

FIGURE 1 Schematic illustration of a counter-current decanter centrifuge with the cylindical length L_{cyl}, the conical length L_{con}, the pool depth h_{p}, the cone angle α, and the bowl radius R_{bo}. The discretization of the decanter centrifuge is depicted for one compartment c with incoming suspension flow $\dot{V}_{c-1}$, outgoing suspension flow $\dot{V}_{\mathrm{c}}$, flow of settled particles $\dot{V}_{\mathrm{sep},c}$, incoming sediment flow $\dot{V}_{\mathrm{sed},c+1}$, and outgoing sediment flow $\dot{V}_{\mathrm{sed},c}$. The illustration focuses on relevant material functions. Further details regarding discretization can be found in Gleiß et al.[3,32] and Menesklou et al.[4]

Lerche et al.[38] and Zhai et al.[39] While this methodology allows for determining the hindered settling velocity on a smaller scale, it may not accurately depict the settling behavior in a decanter centrifuge. This is discussed further in Section 2.3.

The sediment formation process of compressible materials is described by further discretizing the built-up sediment in the radial direction.[3,4] The solids volume fraction of the sediment $\phi_{v,\mathrm{sed}}$ is calculated in each discrete sediment layer using a power law according to Green et al.[40]:

$$\phi_{v,\mathrm{sed}} = \phi_{v,\mathrm{gel}} \left(1 + \frac{p_\mathrm{o}}{p_1}\right)^{\frac{1}{p_2}} \tag{4}$$

with the normal stress p_o and the empirical material parameters p_1 and p_2, which are determined by uniaxial compression experiments.[41] To account for the additional compaction resulting from shearing,[33,42,43] Menesklou et al.[4,44] extended the power law with an additional offset parameter $\phi_{v,\mathrm{sh}}$:

$$\phi_{v,\mathrm{sed}} = \phi_{v,\mathrm{gel}} \left(1 + \frac{p_\mathrm{o}}{p_1}\right)^{\frac{1}{p_2}} + \phi_{v,\mathrm{sh}} \tag{5}$$

The offset parameter $\phi_{v,\mathrm{sh}}$ describes the amount of compaction caused by shearing. While it is possible to determine $\phi_{v,\mathrm{sh}}$ empirically with laboratory shear devices, the shear in these devices is highly simplified compared to the shear in a decanter centrifuge. This makes it challenging to scale the shear compaction derived from shear devices to decanter centrifuges. A direct correlation would require the determination of the actual local shear gradients in the shear devices and the decanter centrifuge in a comparable manner, which is not possible with current methods.[4] Therefore, the shear compaction is neglected in the pure WBM ($\phi_{v,\mathrm{sh}} = 0$).

2.3 | Grey box model

A GBM combines a WBM and a BBM and uses them in conjunction to determine the result. This can have numerous advantages over a pure WBM or BBM, as discussed in Section 4. In general, a GBM can be arranged in either a serial or a parallel structure, which can have a significant impact on the functionality of the model. The optimal structure depends on the specific use case, available data, and quality of the WBM. A parallel GBM is commonly used to address inadequately modeled or missing effects in a WBM by means of a BBM.[10–15,27,45] In this arrangement, the WBM operates independently of the BBM since the BBM only alters the output of the WBM. Consequently, the internal computation of the WBM remains unaffected, which may lead to non-transparent results. Moreover, the final output of a parallel GBM is not constrained by the WBM, allowing for non-physical outputs. There are different ways to combine the WBM and BBM outputs, such as addition or multiplication. Another option is to arrange a GBM in a serial structure. In this arrangement, the BBM feeds intermediate parameters that are either difficult or impossible to measure (e.g., kinetic parameters) to the WBM. In contrast to the parallel structure, the WBM requires the output of the BBM to compute. Due to the physical constraints imposed by the WBM, the output of a serial GBM is always constrained. Another difference is the level of transparency. In the serial GBM, the internal computation of the WBM is also affected by the BBM, leading to a more transparent model in general. The performance of a serial GBM is highly dependent on the quality of the WBM. Figure 2 depicts the model structures examined in this study and the corresponding input and output parameters. The pure BBM directly correlates the selected input parameters (see Section 3.2) with the solids content ϕ. In the parallel GBM, the BBM outputs the residual ϕ_{corr} between the output of the WBM ϕ_{WBM} and the empirical data ϕ_{exp}:

$$\phi_{\mathrm{corr}} = \phi_{\mathrm{WBM}} - \phi_{\mathrm{exp}} \tag{6}$$

thus acting as an estimator of the inaccuracies of the WBM. The final output of the parallel GBM is determined through simple superposition:

$$\phi = \phi_{\mathrm{WBM}} + \phi_{\mathrm{corr}} \tag{7}$$

Menesklou et al.[12] demonstrate that this arrangement can account for local flow effects at deeper pool depths, which improves the accuracy of the predictions. While the authors focus on the interpolation ability, we also evaluate the extrapolation ability in Section 4.2. Before going into details of the serial GBM, it is important to look at the shortcomings of the WBM. As already discussed in Section 2.2, there is currently no reliable method to precisely determine the shear parameter $\phi_{v,\mathrm{sh}}$. Furthermore, the methodology used to obtain the hindered settling function has some shortcomings, such as the relatively narrow (2 mm) measurement cell, which can potentially affect the measurements due to wall effects. In addition, the assumption of spherical particles can result in inaccuracies if the particles are not perfectly spherical. In reality, particles of different sizes can

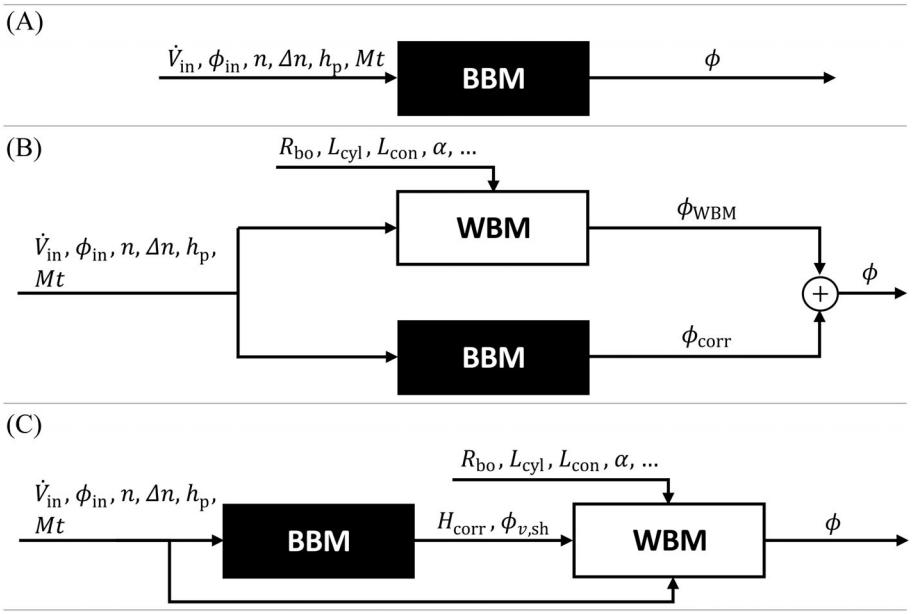

FIGURE 2 Overview of the input and output parameters depending on the modeling structure: (A) pure BBM, (B) parallel GBM and (C) serial GBM. The choice of the input parameters is discussed in Section 3.2.

experience different levels of hindrance. However, the WBM assumes a characteristic hindered settling factor, resulting in uniform hindrance for all particle sizes. This is discussed in more detail by Zhai et al.[39] Additionally, even though the described methodology for deriving the settling velocity is suitable for more ideal conditions like those found in the analytical centrifuge, its validity may be limited in decanter centrifuges due to the more complex flow conditions present. These limitations are thoroughly discussed in Section 4.1. Due to the limitations, we propose incorporating a correction parameter H_{corr} to account for the uncertainties that arise. When combined with Equation (3), we obtain the adjusted hindered settling function:

$$H_{corr} \cdot H(\phi_v) = H_{corr} \cdot r_1 \left(1 - \frac{\phi_v}{r_2}\right)^{r_3} \tag{8}$$

It is important to note that the parameters of the empirical hindered settling function remain unchanged. The serial GBM presented in this study uses a BBM (ANN) to adjust the material functions according to the process conditions. Therefore, the BBM output consists of the difficult to measure shear parameter $\phi_{v,sh}$ (see Equation 5) and the correction factor H_{corr} (see Equation 8). Since labeled targets are required for supervised learning, and the parameters $\phi_{v,sh}$ and H_{corr} cannot be directly measured, they must be identified beforehand through optimization. The parameter identification and supervised training are performed separately. While the parameters $\phi_{v,sh}$ and H_{corr} are not measurable, they are correlated to the measurable solids content. Hence, a Bayesian optimizer[46] (see Section 2.4) is combined with the WBM to identify parameters that minimize the difference between the prediction and the empirical data. The identified parameters are subsequently used for the supervised training process. An alternative option is to use the hybrid model's output as an error signal for identifying the parameters of the BBM.[24,47] However, the computation time of this option is heavily dependent on the complexity of the WBM and is deemed ineffective for this study.

2.4 | Model optimization and evaluation

For a direct comparison of the different model structures shown in Figure 2, it is important to optimize the HPs of the BBM for each model structure (pure BBM, parallel and serial GBM) and evaluate the models in a systematic manner. Since the output parameter of the BBM varies depending on the model structure, it is necessary to optimize the HPs separately for each approach. The search space of the considered HPs, which includes the learning rate, the number of neurons, the number of epochs, the regularization parameter λ, and the activation function, is presented in Table 1. A common practice is to split the available data into training and test sets, with the latter being used for the model evaluation.[29] One drawback of this practice is that the model is only evaluated once on a selected data partition. To reduce the influence of the choice of training and test data on the model performance, k-fold cross validation (CV) is a frequently used method. In k-fold CV, the dataset is partitioned into k folds, with each fold used once as the test set while the rest of the folds are used for training, resulting in k

metrics. Using the RMSE in Equation (1) as the metric, an average score $\overline{\text{RMSE}}_{\text{CV}}$ across all k folds can be calculated:

$$\overline{\text{RMSE}}_{\text{CV}} = \frac{1}{k}\sum_{i}^{k} \text{RMSE}_i \tag{9}$$

Nested CV is an extension of the conventional k-fold CV and combines HP optimization and model evaluation. Using the same data for HP optimization and model evaluation in k-fold CV can lead to overly optimistic results and overfitting because the model has prior knowledge. Varma et al.[48] demonstrate that Nested CV significantly reduces bias in error estimation. To reduce bias, Nested CV incorporates an inner CV specifically for HP optimization and an outer CV for model evaluation. Hereby, the training data of each k_{outer}-fold is further divided into k_{inner}-folds to determine the optimal HPs. The model is subsequently trained with the optimal HPs using the training data from the outer fold and evaluated using the test data from the outer fold. This procedure is repeated for each k_{outer}-fold. While Nested CV is considered more robust than regular k-fold CV, it also requires more computational resources. However, Nested CV is recommended, particularly for small datasets.[26]

In this study, HP optimization and model evaluation were conducted using Nested CV with three k_{inner}-folds and five k_{outer}-folds. For HP optimization, we use a Bayesian optimizer, which approximates the unknown objective function by using a probabilistic surrogate model (Random forest) to iteratively update the beliefs about the objective function. The Bayesian optimizer is efficient since it minimizes the number of evaluations. Furthermore, it is possible to balance the exploration and the exploitation in the search space through an acquisition function, making the Bayesian optimizer a well-suited method for global optimization tasks. A more in-depth description is given by Brochu et al.[46]

TABLE 1 Search space of the Bayesian optimizer. Listed are the range and type of the HPs for the HP optimization.

HP	Range	Type
Number of neurons	[10, 150]	Integer
Number of epochs	[200, 1500]	Integer
Regularization parameter λ	$[10^{-7}, 10^{-1}]$	Log-uniform
Learning rate	$[10^{-3}, 10^{-1}]$	Log-uniform
Activation function	[ReLu, tanh, sigmoid]	Categorical

3 | METHODOLOGY

3.1 | Experimental setup and materials

The experiments were conducted using a laboratory scale decanter centrifuge. Each data point was obtained by conducting three measurements through gravimetric analysis. The inlet solids content was measured shortly before the start of the experiments. Samples of the centrate and sediment were collected in a sample container after the process reached a state of equilibrium and immediately weighted. To cover a wide range of process conditions, significant process parameters were varied. Since the maximum torque of the conveyor's drive is a limiting factor and is reached under different process conditions depending on the material, the range of process parameters differs based on the material. Table 2 presents the geometric parameters of the decanter centrifuge and the process parameters with their respective upper and lower limits. The suspensions used in this study are composed of demineralized water as the continuous phase and either milk calcium (MC), polyvinylchloride (PVC), or limestone (LS) particles as the disperse phase. To stabilize the LS-water and PVC-water suspension, 0.1 wt% sodium pyrophosphate was added to the suspension. Table 3 shows the density and median particle size of the used materials. The suspensions were stirred continuously throughout the experiments using an impeller stirrer to ensure homogeneous suspensions. More detailed information about the particle size distribution and material functions are presented in the Supplementary Materials.

TABLE 2 Geometry of the laboratory scale decanter centrifuge MD80 (Lemitec GmbH) and varied process parameters with their respective upper and lower limits. The g-force G refers to the radius of the bowl.

Geometry parameter	Value	Dimension
Bowl radius R_{bo}	0.04	m
Length cylinder L_{cyl}	0.155	m
Length cone L_{con}	0.16	m
Cone angle α	7	°
Process parameter	**Range**	**Dimension**
Pool depth h_{p}	[0.006, 0.012]	m
Volumetric flow rate $\dot{V}_{\text{in}}$	[5, 80]	L h^{-1}
Rotational speed n	[500, 5500]	min^{-1}
g-force G	[11, 1353]	m s^{-2}
Differential speed Δn	[10, 45]	min^{-1}
Solids content inlet $\phi_{m,\text{in}}$	[4, 15]	wt%

Material parameter	MC	PVC	LS	Dimension
Solid density ρ_{solid}	2310	1400	2700	kg m^{-3}
Median particle size $x_{50,3}$	1.28	2.40	3.68	µm

TABLE 3 Solid density ρ_{solid} and median particle size $x_{50,3}$ of the materials Milk Calcium (MC), Polyvinylchloride (PVC) and Limestone (LS). More information about the materials is presented in the Supplementary Materials.

Index/-	Mt/-	$\phi_{m,in}$/-	$\dot{V}_{in}$/L h^{-3}	Δn/min^{-1}	G/m s^{-2}	h_p/m
1	$X_{1,1}$	$X_{1,2}$	$X_{1,3}$	$X_{1,4}$	$X_{1,5}$	$X_{1,6}$
2	$X_{2,1}$	$X_{2,2}$	$X_{2,3}$	$X_{2,4}$	$X_{2,5}$	$X_{2,6}$
...	...	...	...	...	...	...
I	$X_{I,1}$	$X_{I,2}$	$X_{I,3}$	$X_{I,4}$	$X_{I,5}$	$X_{I,6}$

TABLE 4 Selected features and data structure.

3.2 | Data structure and data scaling

The dataset consists of 238 data points representing a wide range of process conditions. Significant process parameters of a decanter centrifuge are selected as features f, including the inlet volumetric flow rate $\dot{V}_{in}$, the inlet solids mass content $\phi_{m,in}$, the g-force G, the differential speed Δn, the pool depth h_p and the material Mt. As the rotational speed n correlates directly with the g-force, it is not selected as a feature to avoid overweighting. All features are numerical, except for the material, which is categorical. Table 4 illustrates the data structure, where $X_{i,f}$ represents the value of feature f and index i.

To prevent the domination of certain features purely due to different scales, it is important to uniformly scale each feature. Different scaling methods, such as normalization and standardization, are available. As there is no specific distribution within the available data and to preserve the relative relationship between values, each feature is scaled using normalization. Since the material is a categorical feature, a different kind of scaling is needed. One-Hot-Encoding (OHE), is a commonly used method to convert categorical features into numerical values by transforming them into unit vectors, preventing the misinterpretation of an ordinal relationship between them where none exists.[29] Therefore, we use OHE to transform the material into a numerical feature.

4 | RESULTS

4.1 | Prediction accuracy and interpolation ability

For a performance evaluation of the serial GBM, a comparison is made between the serial GBM and the pure WBM in this section. It is important to analyze if any signs of overfitting are present in the predictions made by the serial GBM. Therefore, the interpolation ability is examined in Figure 3 using exemplary cases. As depicted in Figure 3A, the solids content ϕ_m in the centrate decreases as the g-force increases. This is due to the increasing centrifugal forces and the resulting increase in particle settling velocities. With higher solids content in the inlet, the solids content in the centrate increases due to the increased momentum exchange between the solid and liquid phase. Furthermore, more particles are fed into the decanter centrifuge, resulting in a higher sediment and thus a reduced cross-sectional area of the liquid pond. While the WBM accounts for both effects, its predictions deviate from the experimental data, especially at high solids concentrations and low g-forces. The overestimation of the solids content is also apparent in Figure 3C. Here, an increase in the volumetric flow rate leads to a higher solids content, due to the shorter residence time of the particles. While this phenomena is modeled by the WBM, it is striking that the discrepancy between the WBM and experimental data increases at a higher inlet solids content of $\phi_{m,in} = 15$ wt% while the predictions at an inlet solids content of $\phi_{m,in} = 9$ wt% are more in agreement with the experimental results. In addition, the WBM's accuracy decreases as the volumetric flow rate increases. These trends can be further analyzed in Figure 3B,D by examining the predicted values of the parameter H_{corr}. As a point of reference, the target value obtained by optimization (see Section 2.4) is shown, which is the ideal prediction of the BBM. When using the pure WBM, the parameter value is always set to $H_{corr} = 1$, indicating that no adjustment is made to the hindered settling function (see Equation 8). In Figure 3B, the amount of correction required increases as the inlet solids content increases and as the g-force decreases. This indicates that the settling velocity is underestimated, particularly at higher solids contents, which can be partly

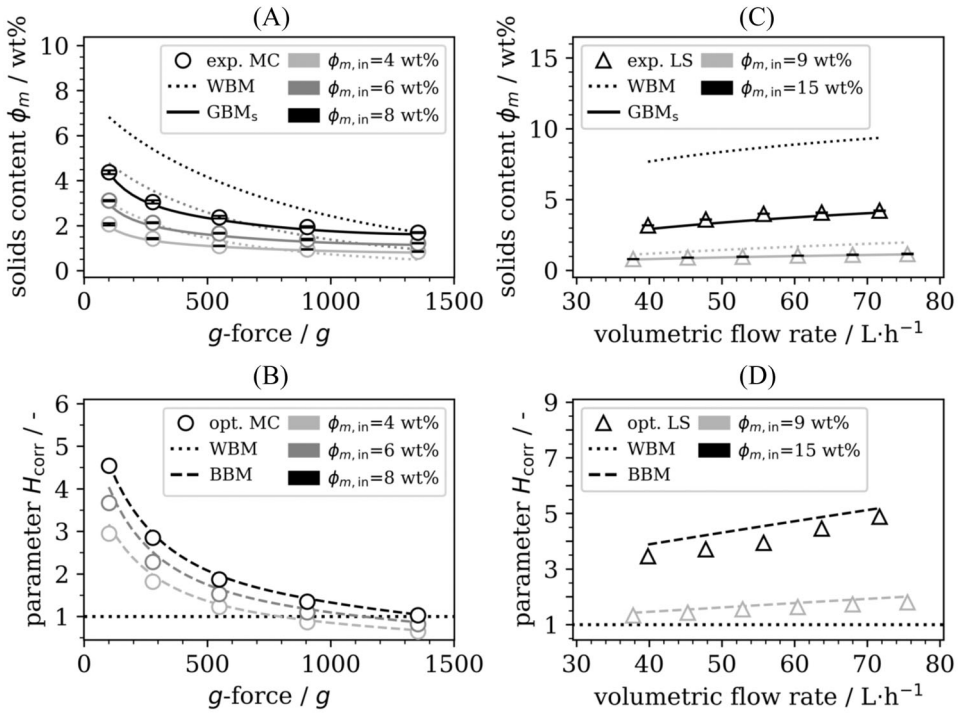

FIGURE 3 Prediction of the solids mass content of the centrate for the material: (A) MC, (C) LS. The result of the serial GBM (GBM$_s$) is compared to that of the WBM. Corresponding prediction of the parameter H_{corr} for the material: (B) MC, (D) LS. For reference, the target value for the parameter H_{corr} obtained by optimization is shown. Constant process parameters in: (A), (B) $\Delta n = 25\,\text{min}^{-1}$, $\dot{V}_{in} = 34\,\text{Lh}^{-1}$, $h_p = 0.012\,\text{m}$, (c), (d) $\Delta n = 25\,\text{min}^{-1}$, $G(\phi_{m,in} = 9\,\text{wt}\%) = 179\,g$, $G(\phi_{m,in} = 15\,\text{wt}\%) = 101\,g$, $h_p = 0.012\,\text{m}$.

explained with the uncertainties arising from the empirical derivation of the hindered settling function, as discussed in Section 2.2. Furthermore, Figure 3D demonstrates that the required correction increases for higher volumetric flow rates, indicating that the discrepancies between WBM and experimental data may not solely caused by the hindered settling function. Another possible cause is the assumption of plug flow within the WBM, whereas the real flow pattern is complex and depends on numerous factors, leading to various approaches for describing the flow pattern inside decanter centrifuges. According to Leung,[49] a thin layer beneath the pool surface is the only part of the pool that moves. The remaining pool is considered to be stagnant. Research studies by Faust et al.[50] and Madsen[51] show that two distinctive flows exist. The upper part of the pool moves towards the weir, whereas the lower part near the inner wall of the bowl moves in the opposite direction. Bai et al.[6] have implemented this flow pattern in a first-principle model, showing good agreement with experimental data. Stahl[33] argues this flow pattern has only been observed at low g-forces and questions its validity at higher g-forces. The accurate description of the flow pattern in decanter centrifuges remains challenging. Although adjusting the hindered settling function does not address the inaccuracies caused by the idealized flow pattern directly, it allows the effects to be considered at a more macroscopic level. Notably, Figure 3A,C demonstrate a significantly improved prediction accuracy of the serial GBM, particularly for higher solids concentrations and throughput rates. In particular, the prediction curves for an inlet solids content of $\phi_{m,in} = 8\text{wt}\%$ and $\phi_{m,in} = 15\text{wt}\%$ are in better agreement with the experimental data than the WBM.

Examining the solids content of the sediment in Figure 4A, the experimental findings demonstrate a rising trend in the solids content with higher g-forces. Increasing centrifugal forces result in greater pressure from the upper sediment layers on the lower layers, leading to a denser and dryer sediment. In Figure 4C, the solids content stays roughly constant as the volumetric flow rate increases. On one hand, an increased number of particles enter the decanter centrifuge resulting in a greater sediment height. On the other hand, the composition of the sediment changes due to the shorter residence time, causing a shift towards larger particles in the cut particle size and thus, reducing the consolidation potential. Although the WBM accounts for these phenomena, there is a noticeable discrepancy between the experimental data and the predictions of the WBM. As discussed in Section 2.2, determining the shear parameter $\phi_{v,sh}$ is challenging, which is why the parameter is set to $\phi_{v,sh} = 0$ in the WBM. As a result, shear compaction of the sediment is neglected within the WBM, causing an underestimation of the solids content, as evidenced in Figure 4A,C. The serial GBM uses the BBM to adjust the material function for sediment compressibility (see Equation 5) with the estimated shear parameter $\phi_{v,sh}$ based on the process conditions. Figure 4B,D demonstrate the output of the BBM at different inlet solid contents, g-forces, and

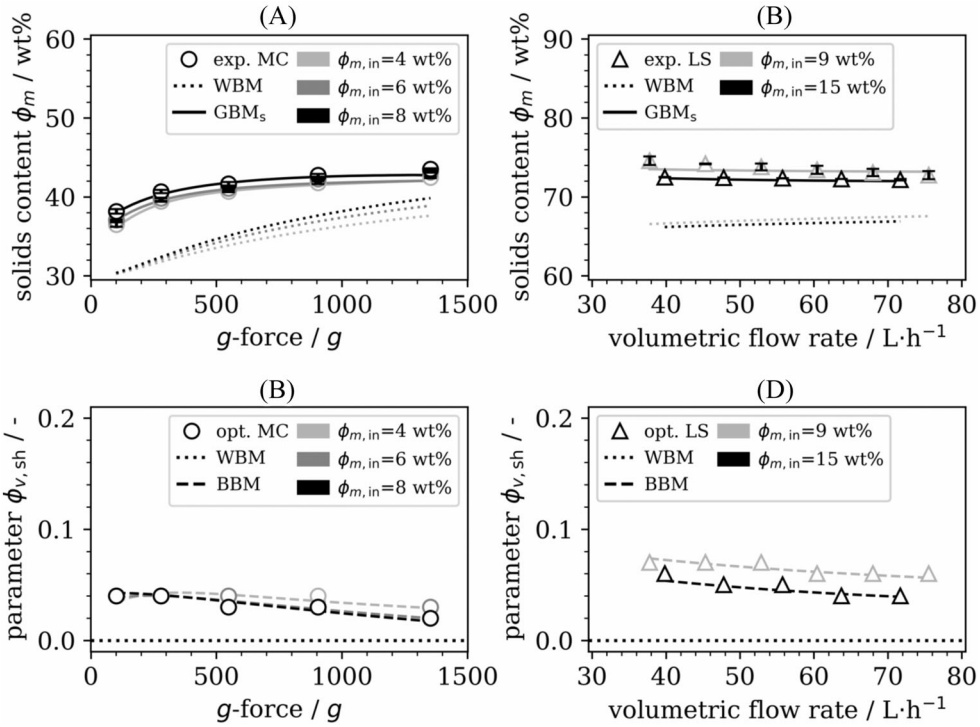

FIGURE 4 Prediction of the solids mass content of the sediment for the material: (A) MC, (C) LS. The result of the serial GBM (GBM$_s$) is compared to that of the WBM. Corresponding prediction of the parameter $\phi_{v,sh}$ for the material: (B) MC, (D) LS. For reference, the target value for the parameter $\phi_{v,sh}$ obtained by optimization is shown. Constant process parameters in: (A), (B) $\Delta n = 25\,\mathrm{min}^{-1}$, $\dot{V}_{in} = 34\,\mathrm{L\,h}^{-1}$, $h_p = 0.012\,\mathrm{m}$, (C), (D) $\Delta n = 25\,\mathrm{min}^{-1}$, $G(\phi_{m,in} = 9\mathrm{wt\%}) = 179\,\mathrm{g}$, $G(\phi_{m,in} = 15\mathrm{wt\%}) = 101\,\mathrm{g}$, $h_p = 0.012\,\mathrm{m}$.

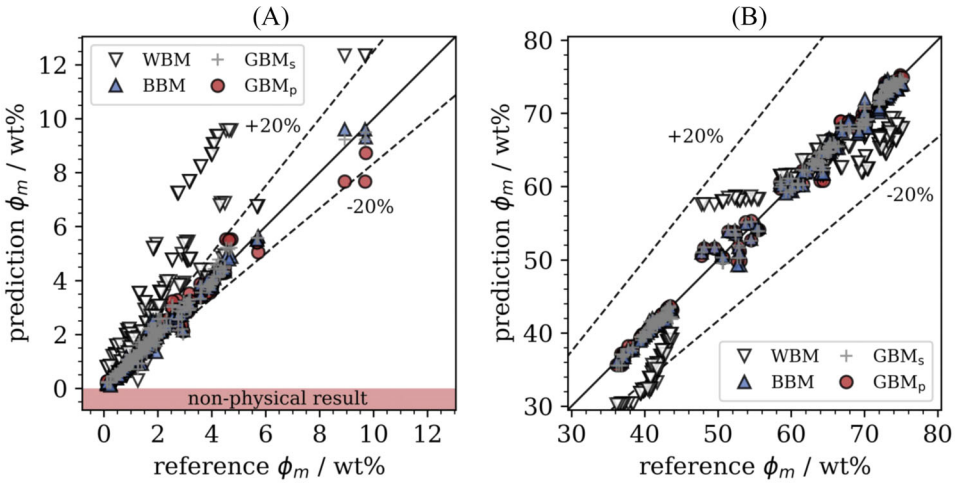

FIGURE 5 Comparison of the experimental data (reference) and the predictions of the pure WBM, the pure BBM, the parallel GBM (GBM$_p$), and the serial GBM (GBM$_s$) for the solids mass content of the: (A) centrate, (B) sediment. The solid diagonal line shows an ideal prediction and the dotted diagonal line shows a relative deviation of +20% and −20%. The red area marks results that are non-physical.

volumetric flow rates. Interestingly, the parameter $\phi_{v,sh}$ is not constant for the regarded materials, suggesting the amount of shear compaction depends on the process conditions. The results, as depicted in Figure 4A,C, highlights the improvement of the model accuracy compared to that of the WBM. The tendency of predicting a less compacted sediment is corrected with the estimated shear parameter. Furthermore, the interpolated data show a plausible trend without any indications of overfitting. This will undergo additional evaluation in Section 4.2.

Figure 5 provides an overview of the serial GBM's performance in relation to alternative model structures. Here, the predictions of the pure BBM, serial and parallel GBM correspond with the test data of each outer fold (see Section 2.4). In Figure 5, it is apparent that the WBM has the tendency to overestimate the solids content of the centrate and to underestimate the solids content of the sediment for previously discussed reasons. When comparing the performance of the data-based model structures, it is noteworthy that all data-driven models deliver a similar performance. This is also evident in Figure 6, which shows the averaged CV score $\overline{\mathrm{RMSE}}_{\mathrm{CV}}$ with the standard deviation of the outer folds. For the WBM, the RMSE of all samples is shown, as CV is only relevant for data-driven methods. Although the WBM has a significantly larger prediction error, it should be noted that a fair comparison with the data-driven models

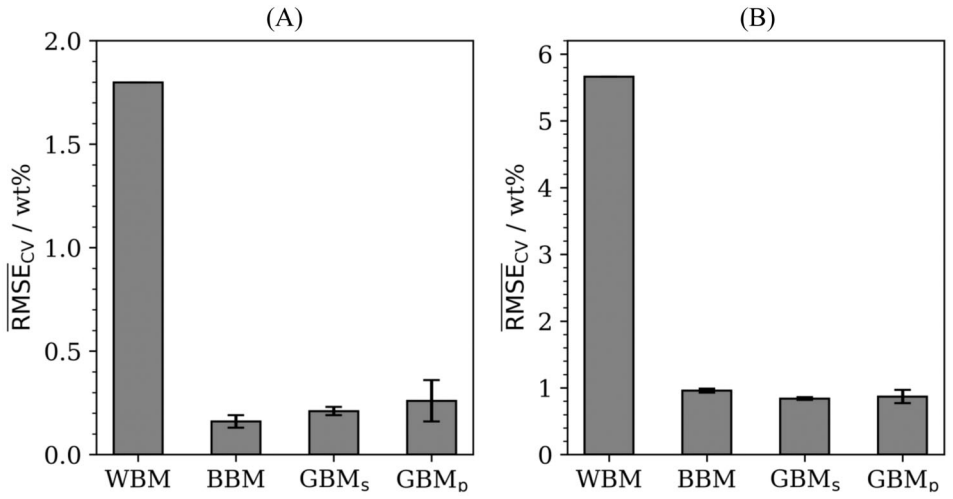

FIGURE 6 Average CV score $\overline{\text{RMSE}}_{\text{CV}}$ with the standard deviation of the outer folds for predicting the solids mass content of the: (A) centrate, (B) sediment. The RMSE of the WBM is shown as a reference.

is not possible since data-driven models require a posteriori knowledge, whereas the WBM uses a priori knowledge for prediction. This enables an initial evaluation of the centrifuge's performance. Nevertheless, a comparison between the WBM and the data-driven approaches can be seen as a benchmark for the accuracy improvement achieved by using a posteriori knowledge. The performance of the BBM and both GBMs is similar with no significant difference in their averaged CV scores. These findings suggests that, on one hand, the available data is significant enough for a pure BBM to perform similarly to a GBM and, on the other hand, the input parameters listed in Table 4 are suitable for predicting the separation outcome in decanter centrifuges. The serial GBM has the lowest standard deviation, which can be interpreted as a sign of good generalization. It is worth noting that the comparison focuses on the prediction quality, and model transparency may also be an important factor when selecting a modeling structure. In this respect, the serial GBM stands out as the most transparent data-driven model, since internal calculations, such as the local kinetics of the separation process and the spatial degree of filling, are available. This allows for a better overall understanding of the process.

4.2 | Extrapolation cases: Comparison of the model structures

The main advantage of a GBM over a pure BBM is the physical background provided by the WBM. In theory, this should lead to a better generalization and extrapolation ability. Particularly the latter is a general weakness of pure BBMs. To evaluate the extrapolation ability of the models, we examine specific cases. Even with Nested CV (see Section 2.4), model extrapolation is not guaranteed, as multiple data points may represent similar process conditions. Data points partitioned as test data may lie inside the trained limits. For ease of distinction, the results obtained by Nested CV are considered to be interpolation, even though technically there is the potential for a minor degree of extrapolation. However, this simplification is justified when comparing the minor degree of extrapolation involved in Nested CV with that of the deliberate extrapolation cases described in the following section.

In the examined extrapolation cases, the training data is restricted to only represent a limited range of *g*-force. The *g*-force was selected as the restricted parameter due to its significance on the separation outcome. As the lower and upper limit of the *g*-force are material specific (see Section 3.1), two training data ranges are defined: data points within the ranges $178g < G < 280g$ for the material LS and $547g < G < 906g$ for the materials PVC and MC are used for training, while the remaining data is held back for testing. This manual training-test split reduces the amount of training data to 101 data points and forces the models to extrapolate when predicting the test data. While the studied cases are specific, they provide a general insight of the extrapolation ability of the models. The HPs of the ANN in the examined model structures are optimized on the entire training data. We do not apply Nested CV in the extrapolation cases due to the present limitations of the training data. Figures 7 and 8 give an overview of the prediction accuracy of the data-driven models for the extrapolated data. Comparing Figures 5 and 7, it is evident that the overall prediction error is significantly higher with the constrained training data. This is to be expected since the number of training data is reduced and the range of process conditions covered by the training data is significantly narrower. The choice of training data does not affect the WBM, and thus, it is not shown here. Figure 7A demonstrates that the constrained training data leads to noticeably poorer performance of

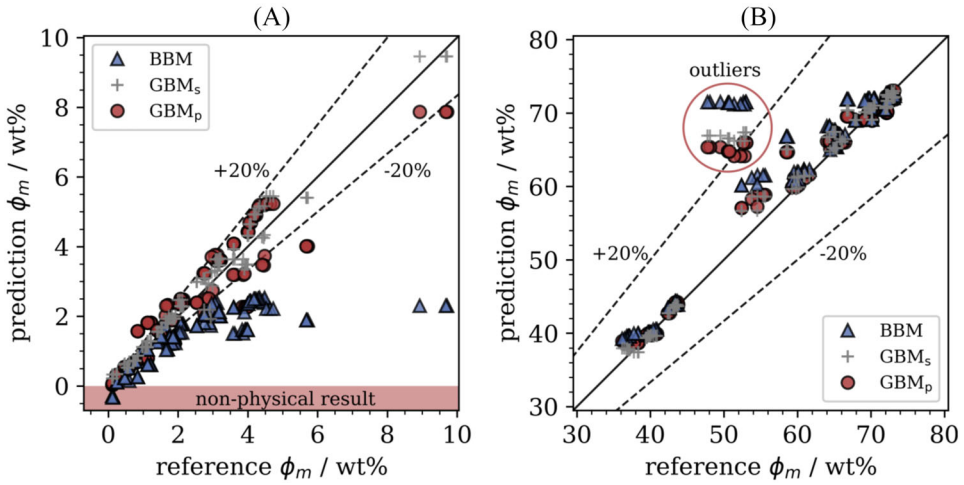

FIGURE 7 Comparison of the experimental data (reference) and predictions of the extrapolated (test) data of the pure BBM, the parallel GBM (GBM_p), and the serial GBM (GBM_s) for the solids mass content of the: (A) centrate, (B) sediment. The solid diagonal line shows an ideal prediction and the dotted diagonal line shows a relative deviation of +20% and −20%. The red area marks results that are non-physical. Extreme process conditions ($G = 11\,g$) are highlighted with a red circle.

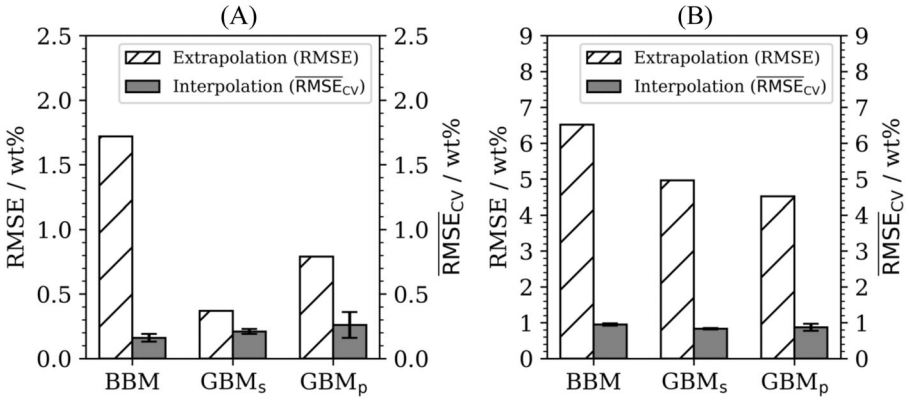

FIGURE 8 RMSE for predicting the extrapolation cases for the: (A) centrate, (B) sediment. The average CV score $\overline{RMSE}_{CV}$ is shown for easier comparison.

the pure BBM when predicting the solids content of the centrate. The pure BBM even predicts negative solids contents due to the absence of physical boundaries. In contrast, the serial GBM proves to be reliable despite the limited training data, highlighting the advantages of this model structure. The WBM acts as a stabilizer leading to more accurate extrapolation. Negative results for the solids content are not possible due to the constraints imposed by the WBM. The parallel GBM performs noticeably better than the pure BBM but worse than the serial GBM. Interestingly, the differences between the models are less pronounced when predicting the solids content of the sediment, as observed in Figure 7B. Here, the limited training data has a smaller impact on the predictions, except for a few outliers marked in Figure 7B. It is worth noting that these outliers were collected under similar process conditions, specifically at low *g*-forces ($G = 11\,g$) with the material LS. The sample collection proved challenging due to slow sediment build-up, requiring a significant amount of time to accumulate sufficient sediment for transport. These extreme process conditions pose a challenge for all models to extrapolate. However, it is worth noting that these low *g*-forces are generally technically irrelevant. The results presented in Figure 8 allow for further discussion of the extrapolation ability of the models. The difference between the Nested CV score (see Figure 6) and the extrapolation score can be interpreted as the model's reliance on the training data. A larger difference between the two scores indicates a greater impact of the training data on the prediction error. For ease of comparison, the Nested CV score is also shown in Figure 8. Comparing the scores leads to the conclusion that the constrained training data has the greatest impact on the pure BBM, as the RMSE is significantly higher for the extrapolation cases. The serial GBM's prediction error for the solids content of the centrate is similar for extrapolation and Nested CV, which highlights the generalization ability of the serial GBM. As depicted in Figure 8B, the prediction error for the solids content of the sediments gets noticeably larger for all modeling approaches for the extrapolation cases. However, the outliers representing extreme process conditions mentioned earlier largely contribute to the prediction error.

While Figures 7 and 8 give a general impression of the extrapolation ability of the models, it is important to examine them in more detail to further rule out overfitting. The exemplary prediction curves in Figure 9 allow for further discussion. Here, the models must predict the

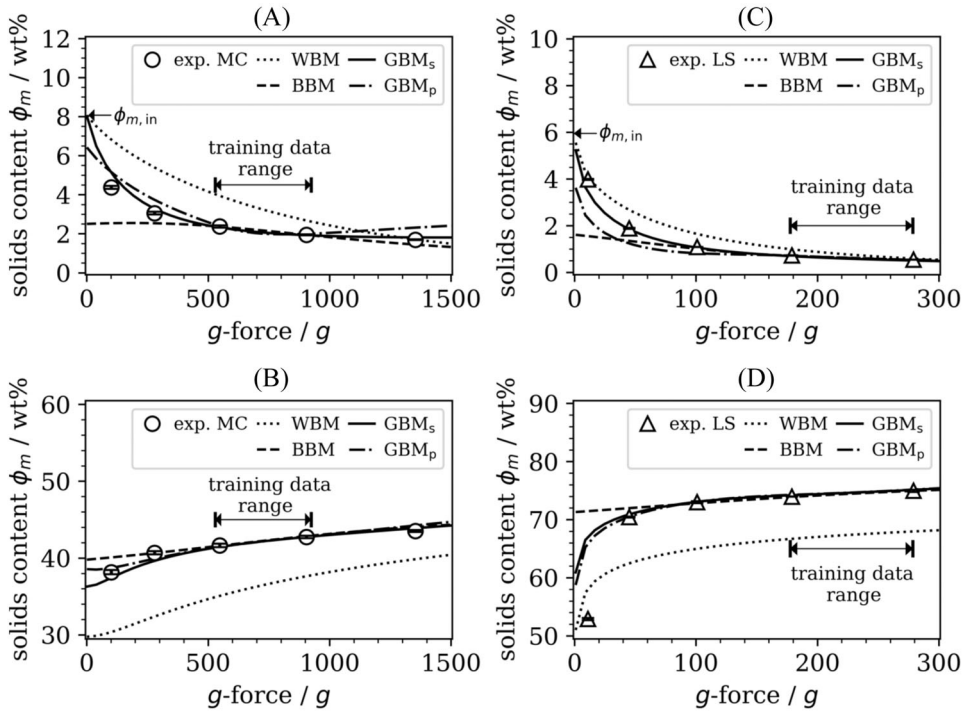

FIGURE 9 Comparison of the extrapolated data for the: (A) centrate and the material MC, (B) sediment and the material MC, (C) centrate and the material LS, (D) sediment and the material LS. The depicted range covered by the training data allows for differentiating between interpolation and extrapolation. Constant process parameters in: (A), (B) $\phi_{m,\mathrm{in}} = 8\,\mathrm{wt\%}$, $\Delta n = 25\,\mathrm{min}^{-1}$, $\dot{V}_{\mathrm{in}} = 34\,\mathrm{L\,h}^{-1}$, $h_p = 0.012\,\mathrm{m}$, (c), (d) $\phi_{m,\mathrm{in}} = 6\,\mathrm{wt\%}$, $\Delta n = 25\,\mathrm{min}^{-1}$, $\dot{V}_{\mathrm{in}} = 34\,\mathrm{L\,h}^{-1}$, $h_{\mathrm{p}} = 0.012\,\mathrm{m}$.

operation under process conditions that are not represented in the constricted training data. To illustrate the limited information the available training data contains, the range of the training data is displayed in Figure 9. While all data-based models make similar predictions within the training data range, it is striking that the pure BBM struggles to make reliable predictions beyond this range. In Figure 9, the pure BBM predicts a nearly linear trend in the solids content with respect to the *g*-force, which is not in accordance with the experimental data. Furthermore, Figure 9A shows that the pure BBM predicts a decreasing trend in the solids content of the centrate at lower *g*-forces, which is implausible as lower centrifugal forces should result in less particle settling. Although the pure BBM may learn this correlation with additional training data, it highlights the shortcomings of purely data-driven models. Due to the insufficient information provided by the sparse training data and the lack of physical information, the pure BBM is unable to reliably extrapolate in the examined cases. This is a common issue among purely data-driven models. In contrast, the serial GBM shows a physically correct trend that is consistent with the experimental data. In Figure 9A,C, the solids content of the centrate increases at lower *g*-forces and approaches the inlet solids mass content $\phi_{m,\mathrm{in}}$. This behavior is expected as very low *g*-forces should result in an unpurified centrate. The parallel GBM performs better than the pure BBM, but there are some inconsistencies. From Figure 9A, it is evident that the parallel GBM predicts an increasing solids content of the centrate at *g*-forces $G > 800g$, which is contrary to the theory. Additionally, although the solids content increases at lower *g*-forces in Figure 9A,C, it does not reach the inlet solids content as anticipated. The differences between the models are less pronounced when predicting the solids content of the sediment, as depicted in Figure 9B,D. This can be explained with the general trend of the data. The centrate is generally more sensitive to the varied process parameters for the examined materials and process conditions. Moreover, the materials compress mainly at low *g*-forces. At higher *g*-forces, the compressive potential is approached, leading to a more or less linear trend of the data, which is comparatively easier to predict. Nevertheless, in the examples shown in Figure 9B,D, both GBMs perform better than the pure BBM, especially at lower *g*-forces. These findings confirm the statement that pure BBMs are unreliable for extrapolation. In the application case of a decanter centrifuge, the examined BBM requires an adequate amount of data representing the full range of process conditions for reliable predictions. In contrast, the presented serial GBM requires less data as a result of the a priori knowledge provided by the WBM and shows a significantly better extrapolation performance. Although the examined cases of extrapolation are specific, they clearly demonstrate the structural advantages of the serial GBM.

5 | CONCLUSION

This paper explores the efficacy of hybrid modeling as a strategy for accurately predicting the separation

performance of decanter centrifuges. A systematic comparison of the interpolation and extrapolation ability of various modeling approaches, including a pure white box model (WBM), a pure black box model (BBM) and both a serial and a parallel grey box model (GBM), underscore the importance of the model structure. The findings highlight the advantages of the introduced serial GBM, which integrates an artificial neural network (ANN) with a real-time first-principle model to predict unknown material parameters. Notably, while the data-driven models exhibit comparable prediction accuracy and interpolation ability with sufficient training data, the serial GBM excels in extrapolation, providing more reliable predictions for unseen process conditions.

Overall, the results demonstrate the potential of hybrid modeling as a valuable tool for accurately predicting the separation result of decanter centrifuges. This enables the optimization of the operation to achieve a cost-effective and sustainable separation process.

In terms of future research, using the serial GBM for scale-up purposes by predicting separation performance of larger scale machines through laboratory scale training would allow for further exploration of its extrapolation ability. Additionally, considering its real-time capability and high prediction accuracy, the presented serial GBM holds promise as a foundation for model predictive control of decanter centrifuges.

6 | PLS

Designing solid bowl centrifuges, including decanter centrifuges, is challenging due to dynamic events within the apparatus, such as particle settling, sediment build-up, and consolidation. Current methods rely on simplified models, often leading to inaccuracies. Therefore, manufacturers must perform time-intensive pilot scale experiments to derive their own correction factors. The increasing computing power has led to a growing interest in alternative modeling strategies, such as hybrid models. Grey box models (GBMs) are a combination of mechanistic white box models (WBM) and data-driven black box models (BBM). The WBM and BBM can be arranged in various ways, either in parallel or in series, with the optimal arrangement depending on the specific application. To improve the process design of decanter centrifuges, we conducted a comprehensive comparison of different modeling strategies, including a pure BBM, a parallel GBM and a serial GBM. Our proposed serial GBM includes an artificial neural network and a mechanistic model that divides the helical screw channel of the decanter centrifuge into multiple compartments. The neural network feeds unknown material parameters into the mechanistic multi-compartment model to better reflect the real material behavior. This approach outperforms other data-driven modeling strategies in terms of extrapolation, prediction ability, model transparency, and efficiency while also enabling a better comprehension of the separation process in decanter centrifuges.

AUTHOR CONTIRBUTIONS

Ouwen Zhai: Conceptualization; methodology; formal analysis; investigation; writing – original draft preparation; writing – review and editing; validation; visualization. **Niklas Ehret:** Investigation. **Frank Rhein:** Writing – review and editing. **Marco Gleiss:** Funding acquisition; project administration; supervision; writing – review and editing.

ACKNOWLEDGMENTS

This research was funded by the German Federation of Industrial Research Associations (AiF Arbeitsgemeinschaft Industrieller Forschungsvereinigungen Otto von Guericke e.V. 21638N) and the Federal Ministry for Economic Affairs and Climate Action (BMWk) within the AiF-IGF project. Open Access funding enabled and organized by Projekt DEAL.

CONFLICT OF INTEREST STATEMENT

The authors declare no conflicts of interest.

DATA AVAILABILITY STATEMENT

To ensure reliability and reproducibility, numerical data from Figures S3–S9 are tabulated in the Supplementary Materials, along with information about the discretization, and the experimental data used as input for the neural network. Supplementary Figures and corresponding numerical data provide additional information about the examined materials, including particle size distribution, hindered settling function, and compression function.

ORCID

Ouwen Zhai https://orcid.org/0009-0008-5250-7010

REFERENCES

[1] C. Ambler, *Chem. Eng. Prog.* **1952**, *48*, 150.
[2] S. Hammerich, M. Gleiß, H. Nirschl, *ChemBioEng Rev.* **2019**, *6*, 108.
[3] M. Gleiss, S. Hammerich, M. Kespe, H. Nirschl, *Chem. Eng. Technol.* **2018**, *41*, 19.
[4] P. Menesklou, H. Nirschl, M. Gleiss, *Sep. Purif. Technol.* **2020**, *251*, 117287.
[5] P. Menesklou, T. Sinn, H. Nirschl, M. Gleiss, *Minerals* **2021**, *11*, 229.
[6] C. Bai, H. Park, L. Wang, *Sep. Purif. Technol.* **2021**, *263*, 118408.
[7] C. Bai, H. Park, L. Wang, *Minerals* **2022**, *12*, 1288.

[8] A. Jiménez, G. Beltrán, M. P. Aguilera, M. Uceda, *Sens. Actuators, B* **2008**, *129*, 985.
[9] A. Jiménez Marquez, M. P. Aguilera Herrera, M. Uceda Ojeda, M. G. Beltrán, *J. Food Eng.* **2009**, *95*, 135.
[10] M. Stosch, R. Oliveira, J. Peres, S. Feyo de Azevedo, *Comput. Chem. Eng.* **2014**, *60*, 86.
[11] D. S. Lee, P. A. Vanrolleghem, J. M. Park, *J. Biotechnol.* **2005**, *115*, 317.
[12] P. Menesklou, T. Sinn, H. Nirschl, M. Gleiss, *Minerals* **2021**, *11*, 755.
[13] G. M. Bollas, S. Papadokonstadakis, J. Michalopoulos, G. Arampatzis, A. A. Lappas, I. A. Vasalos, A. Lygeros, *Chem. Eng. Process. Process Intensif.* **2003**, *42*, 697.
[14] Q. Xiong, A. Jutan, *Chem. Eng. Sci.* **2002**, *57*, 1027.
[15] J. Peres, R. Oliveira, S. Feyo de Azevedo, *Comput. Chem. Eng.* **2001**, *25*, 783.
[16] A. Bazaei, V. J. Majd, *J. Process Control* **2003**, *13*, 819.
[17] A. Azarpour, T. Borhani, S. R. Wan Alwi, Z. A. Manan, I. A. Mutalib M, *Chem. Eng. Res. Des.* **2017**, *117*, 149.
[18] O. Kahrs, W. Marquardt, *Chem. Eng. Process. Process Intensif.* **2007**, *46*, 1054.
[19] O. Kahrs, W. Marquardt, *Comput. Chem. Eng.* **2008**, *32*, 694.
[20] R. Oliveira, *Comput. Chem. Eng.* **2004**, *28*, 755.
[21] H. C. Aguiar, R. M. Filho, *Chem. Eng. Sci.* **2001**, *56*, 565.
[22] C. A. O. Nascimento, R. Giudici, N. Scherbakoff, *J. Appl. Polym. Sci.* **1999**, *72*, 905.
[23] X. Wang, J. Chen, C. Liu, F. Pan, *Chem. Eng. Res. Des.* **2010**, *88*, 415.
[24] P. Georgieva, M. J. Meireles, S. Feyo de Azevedo, *Chem. Eng. Sci.* **2003**, *58*, 3699.
[25] D. C. Psichogios, L. H. Ungar, *Ind. Eng. Chem. Res.* **1991**, *30*, 2564.
[26] F. Rhein, L. Hibbe, H. Nirschl, *Eng. Computation* **2023**, *3*, 217.
[27] Y. Chen, M. Ierapetritou, *AIChE J.* **2020**, *66*, e16996.
[28] W. Bradley, J. Kim, Z. Kilwein, L. Blakely, M. Eydenberg, J. Jalvin, C. Laird, F. Boukouvala, *Comput. Chem. Eng.* **2022**, *166*, 107898.
[29] A. Géron, *Hands-on machine learning with Scikit-Learn, Keras and TensorFlow: Concepts, tools, and techniques to build intelligent systems*, O'Reilly Media, Inc, Sebastopol **2019**.
[30] A. E. Hoerl, R. W. Kennard, *Technometrics* **1970**, *12*, 55.
[31] C. C. Aggarwal, *Neural Networks and Deep Learning*, 2nd ed., Springer International Publishing and Imprint Springer, Cham **2023**.
[32] M. Gleiss, S. Hammerich, M. Kespe, H. Nirschl, *Chem. Eng. Sci.* **2017**, *163*, 167.
[33] W. H. Stahl, *Industrie-Zentrifugen: Maschinen- & Verfahrenstechnik*, 1st ed., DrM Press, Männedorf **2004**.
[34] A. D. Stickland, Solid-liquid Separation in the Water and Wastewater Industries. Doctoral dissertation. Melbourne, The University of Melbourne. **2005**.
[35] L. Spelter, Abtrennung und Klassierung kolloidaler Partikel in Zentrifugen: Experimenteller Nachweis und Modellierung der Sedimentation in halbkontinuierlichen Vollmantelzentrifugen. Doctoral dissertation. Karlsruhe, Karlsruhe Institute of Technology. **2012**.
[36] G. G. Stokes, *Mathematical and Physical Papers*, Cambridge University Press, Cambridge **1880**.
[37] A. S. Michaels, J. C. Bolger, *Ind. Eng. Chem. Fund.* **1962**, *1*, 24.
[38] D. Lerche, *J. Dispersion Sci. Technol.* **2002**, *23*, 699.
[39] O. Zhai, H. Baust, M. Gleiß, H. Nirschl, *Chem. Ing. Tech.* **2023**, *95*, 189.
[40] M. D. Green, M. Eberl, K. A. Landman, *AIChE J.* **1996**, *42*, 2308.
[41] H. Reinach, Gleichgewicht and Kinetik der Preßentfeuchtung im Zentrifugalfeld einer Becherzentrifuge und in einer Stempelpresse dargestellt an einem stark kompressiblen Kaolinschlamm. Doctoral dissertation. Karlsruhe, University of Karlsruhe. **1992**.
[42] G. M. Channell, C. F. Zukoski, *AIChE J.* **1997**, *43*, 1700.
[43] A. Erk, Rheologische Eigenschaften feindisperser Suspensionen während ihrer Fest-Flüssig-Trennung in Filtern und Zentrifugen. Doctoral dissertation. Karlsruhe, University of Karlsruhe. **2006**.
[44] P. Menesklou, Entwicklung eines hybriden Simulationsmodells zur Optimierung des Betriebsverhaltens von Dekantierzentrifugen. Doctoral dissertation. Karlsruhe, Karlsruhe Institute of Technology. **2022**.
[45] S. Safari, F. Shabani, D. Simon, *Aerosp. Sci. Technol.* **2014**, *39*, 465.
[46] E. Brochu, V. M. Cora, N. Freitas, A tutorial on bayesian optimization of expensive cost functions, with application to active user modeling and hierarchical reinforcement learning.
[47] C. Azevedo, R. Lee, R. M. C. Portela, M. Stosch, R. Oliveira, *Artificial Neural Networks in Chemical Engineering*, Nova Science Publishers, Inc., New York **2017**, p. 229.
[48] S. Varma, R. Simon, *BMC Bioinf.* **2006**, *7*, 91.
[49] W. W. Leung, *Industrial Centrifugation Technology*, McGraw-Hill, New York **1998**.
[50] T. Faust, W. Gösele, *Chem. Ing. Tech.* **1985**, *57*, 698.
[51] B. Madsen, *Int. Chem. Eng. Symp. Ser.* **1989**, *113*, 301.

SUPPORTING INFORMATION

Additional supporting information can be found online in the Supporting Information section at the end of this article.

How to cite this article: O. Zhai, N. Ehret, F. Rhein, M. Gleiss, *J. Adv. Manuf. Process.* **2024**, e10179. https://doi.org/10.1002/amp2.10179